PHYSICAL REVIEW E **88**, 010702(R) (2013)

Sedimentation-induced tether on a settling vesicle

Gwenn Boedec,[1,*] Marc Jaeger,[2] and Marc Leonetti[1,†]
[1]*Aix Marseille Université, CNRS, Centrale Marseille, IRPHE UMR 7342, 13384 Marseille, France*
[2]*Aix Marseille Université, CNRS, Centrale Marseille, M2P2 UMR 7340, 13451 Marseille, France*
(Received 31 August 2012; published 8 July 2013)

Destabilization of soft interfaces into thin cylindrical filaments under external stresses is ubiquitous and is generally the first step toward breakup. We show that such filaments, called tethers, emerge from a vesicle subjected to gravity. Contrary to the pendant drop experiment, we demonstrate that the bending rigidity, a specific membrane property of vesicles, ensures the tethers reach a stationary state. Moreover, unlike point-like force experiments, we show that the family of shapes is continuous.

DOI: 10.1103/PhysRevE.88.010702 PACS number(s): 87.16.D−, 47.15.G−, 47.57.ef, 82.70.Uv

Understanding the behavior of deformable particles such as drops, cells, or polymers under flow is a universal problematic arising in biological processes, fluid mechanics of suspensions, and physics of soft matter. As in many other systems, there is a coupling between the shape and dynamics at the microscopic (particle) scale and the global behavior, especially nonlinearities at the macroscopic (suspension) scale. A specificity of deformable particle suspensions is that nonlinearities are also present at the microscopic scale, resulting from the interplay between the deformability of the particle and the characteristics of the flow. These nonlinearities are even more manifest in the large deformation regime, which can generally be easily triggered on such particles, either by the application of focused stresses (point-like forces) or by the application of a stress exceeding a critical value. These regimes are characterized by the presence of multiple length scales [1] ranging from the system size to a microscopic scale several orders of magnitude smaller, up to geometrical singularities [2,3]. Understanding these large deformation regimes is crucial not only for applicative problematics where the stability of the interface controls the size of droplets produced after breakup but also for biological problematics such as the formation of a thin tube of membrane, which are observed in the Golgi apparatus, in tunneling nanotubes [4], and during the rolling motion of leukocytes [5]. Beyond their diverse physical origins, the underlying problematics of emerging long finger-like shapes are the same: the real interface shape, its dynamics, and its stability. Some remarkable features are recovered whatever the system, at least transiently: a marked neck between the quasispherical deformable particle and its tail, whose evolution controls the integrity of the deformable particle, and the appearance of pearls along the tail are common examples observed on drops or on vesicles.

Particular difficulties in understanding such situations are both the large range of scales involved and the fast dynamics preceding pearl formation or breakup. Using highly viscous fluids can lead to very long filaments [1], and the addition of minute amounts of polymers in solution can lead to a substantial delay of the pinch-off [6]. However, the filament will eventually breakup. This breakup is associated with constant evolution of the shape (thinning of the filament and growth of unstable perturbations), leading to a zero radius at the point of pinch. One way to reach the shape stationarity is a phase transition of bulk materials such as induced by the well-known electrospinning of polymer melts [7]. In this Rapid Communication, we demonstrate that a second way involves only the interfacial mechanical properties while preserving the system fluidity to obtain a thin stationary filament. We consider a vesicle, a typical example of a deformable particle, which is a drop of fluid enclosed by a self-organized fluid membrane. A vesicle differs markedly from a drop by its membrane properties: surface incompressibility (also called fixed-area constraint) and resistance to bending instead of only the surface tension for drops. If membrane integrity prevents any breakup, it does not imply the shape stationarity. On the contrary, we show that the filament stationarity is due to bending energy and not to the fixed-area constraint, as a first intuitive statement might conclude.

Vesicles have been extensively studied as a model system [8,9] to understand red blood cell behavior under flow [10], especially in shear flow [11,12] or wall-induced migration [13,14]. They have also been used to understand the formation of a thin tube of membranes [15–22] under the application of point-like force. An important result is that, for a membrane with a fixed tension σ, the point-like force must exceed a critical value $f_c = 2\pi\sqrt{2\sigma\kappa}$ to pull a tube out of the membrane [23,24], with κ being the bending modulus of the membrane (typical value $\kappa \sim 20k_BT$). However, the assumption of fixed tension necessitates the connection of the membrane to an area reservoir, be it excess area stored in thermal fluctuations of the membrane or area aspirated in a pipette. For freely suspended vesicles under flow, this assumption is no longer verified, but membrane tubes are still observed experimentally in shear [25], acoustic-driven [26], elongational [27,28], and settling [29] flows. Recent progress in numerical modeling of vesicles has permitted simulations of transient tubes in shear [12] and elongational [30] flows.

We study this effect by investigating the formation of a membrane tube on a settling vesicle, a prototypal configuration (no imposed external flow) where Newtonian drops undergo large deformations, with the development of a filament at the rear of the drop leading to breakup. In the case of a vesicle, a tether is pulled by the settling-induced stresses (see Fig. 1), and we show that the elongation of the tether reaches a plateau, leading to the stationarity of the system. There are continuous families of stationary shapes (see Figs. 2 and 3) which connect

*boedec@irphe.univ-mrs.fr
†leonetti@irphe.univ-mrs.fr

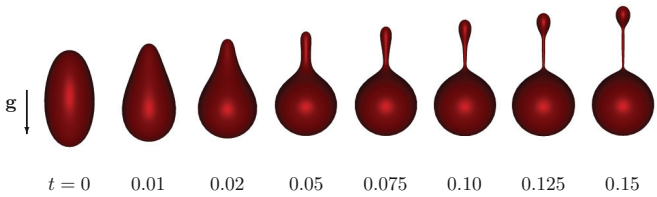

FIG. 1. (Color online) Formation of a tether on a settling vesicle starting from a prolate shape ($\Delta = 0.97, \mathrm{Bo} = 490$). Time is made dimensionless by the viscous one, $\eta R_0^3/\kappa$.

quasispherical shapes to fully developed tethers, with aspect ratios up to 200. The transient dynamics of the formation of the tether, which can lead to the formation of pearls, observed both in experiments [29] and in our simulations, is beyond the scope of this Rapid Communication, but the analysis presented here is a necessary first step toward it. In particular, the preliminary results indicate that pearls are only transient, disappearing after a while to reach the stationary state described here.

When no hydrodynamical stresses are present, the vesicle shape results from the minimization of the free energy F of the membrane, which is usually given by the energy of Helfrich together with the constraint of fixed volume and area ensured by the use of the Lagrange multipliers γ, p:

$$F = F_m + \int_V p dV = \int_S (2\kappa H^2 + \gamma) dS + \int_V p dV \quad (1)$$

with H being the surface mean curvature. At equilibrium, the Lagrange multipliers are actually constant over the whole membrane and thus constrain the total area and volume. For a settling vesicle, flows will exert hydrodynamical stresses on the membrane inducing the deformation of the vesicle. Thus, γ and p are no longer constant and ensure the local preservation of area and volume. These geometric constraints have crucial consequences on the dynamics of a vesicle: since both the enclosed volume and the membrane area are fixed, a spherical vesicle cannot deform, whatever the external stresses are. The geometrical deformability is measured by the dimensionless deviation Δ of the area A with respect to the area of the sphere having the same volume V. With $R_0 = (3V/4\pi)^{1/3}$, Δ, called the excess area, is given by $A = (4\pi + \Delta)R_0^2$.

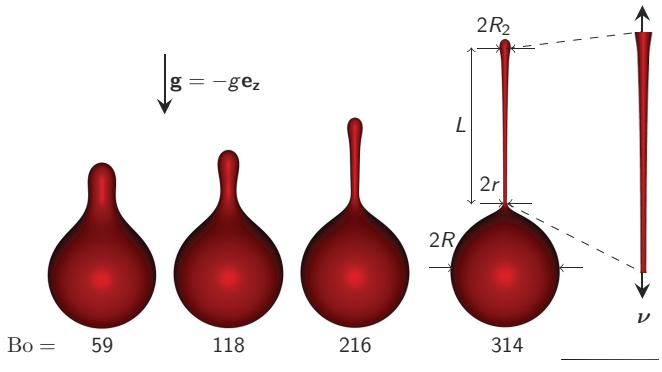

FIG. 2. (Color online) The shape evolves continuously from a pear-like shape [31,32] to a tethered shape, with increasing forcing represented by an increasing Bond number (Bo) with a fixed excess area ($\Delta = 0.93$).

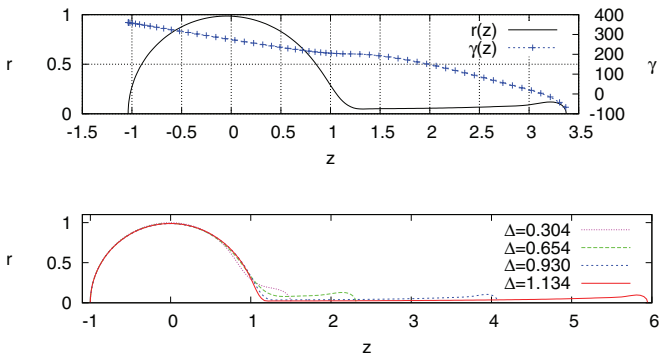

FIG. 3. (Color online) (top) Profile $r(z)$ of the stationary shape for ($\Delta = 0.93, \mathrm{Bo} = 304$), along with the evolution of the Lagrange multiplier $\gamma(z)$. (bottom) Comparison of four different stationary profiles for a fixed Bond number ($\mathrm{Bo} = 304$) and with a varying excess area. r and γ are made dimensionless by R_0 and κ/R_0^2, respectively.

The hydrodynamical fields are described within the Stokes approximation ($\eta \Delta \boldsymbol{v}^{i,e} - \nabla \bar{p}^{i,e} = \boldsymbol{0}$) with the continuity condition ($\nabla \cdot \boldsymbol{v}^{i,e} = 0$), where $\boldsymbol{v}$ is the velocity, $\bar{p}^{i,e} = p^{i,e} + \rho^{i,e} g z$ is the pressure modified to include the contribution of the buoyancy, ρ is the fluid density, η is the dynamic viscosity, g is gravity, and the superscripts i and e stand for the internal and the external fluids, respectively. These hydrodynamical fields are coupled to the membrane by the conditions of continuity of the velocity field across the membrane [$\boldsymbol{v}^{\boldsymbol{i}}(\boldsymbol{x}) = \boldsymbol{v}^{\boldsymbol{e}}(\boldsymbol{x}) = \partial_t \boldsymbol{x}$], the constraint of surface incompressibility of the velocity field [$\nabla_s \cdot \boldsymbol{v}(\boldsymbol{x}) = 0$], and the mechanical equilibrium of the membrane ($[\overline{\overline{\boldsymbol{\sigma}}}^{e} - \overline{\overline{\boldsymbol{\sigma}}}^{i}] \cdot \boldsymbol{n} + \boldsymbol{f^m} - (\delta \rho g z)\boldsymbol{n} = \boldsymbol{0}$), where $\boldsymbol{x}$ is the position of the membrane, $\overline{\overline{\boldsymbol{\sigma}}} = -\bar{p}\overline{\overline{\boldsymbol{I}}} + \eta(\nabla \boldsymbol{v} + \nabla^T \boldsymbol{v})$ is the modified fluid stress tensor, $\boldsymbol{n}$ is the outward pointing normal vector to the interface, and $\delta\rho = \rho^i - \rho^e$ is the difference of the density between the inside and outside. $\boldsymbol{f^m} = -\delta F_m/\delta \boldsymbol{x}$ is the density of force due to shape changes:

$$\boldsymbol{f^m} = \{2\gamma H - \kappa[2\Delta_s H + 4H(H^2 - K)]\}\boldsymbol{n} + \nabla_s \gamma, \quad (2)$$

with Δ_s being the Laplace-Beltrami operator over the surface and K being the Gaussian curvature.

Numerics. The system is closed by requiring that the velocity field induced by the settling and the deformation of the vesicle vanish at infinity: $\boldsymbol{v}^{\boldsymbol{e}}_{|\boldsymbol{x}| \to \infty} \to 0$. To solve this problem, we use a numerical method [31] based on the boundary element method for the computation of Stokes flows, modified to deal with the computation of membrane forces as well as with the treatment of the constraint of surface divergence free of the velocity field. Even in the large deformation regime studied here, our method fulfills the constraint of surface incompressibility up to a precision of 10^{-8} and preserves the total area and volume up to a relative precision of 10^{-5}.

Results. The dynamics of the system depends on two dimensionless control parameters (no viscosity contrast between the inside and outside here): the excess area Δ and the Bond number $\mathrm{Bo} = \delta\rho g R_0^4/\kappa$.

In the limit of quasispherical shapes ($\Delta \sim 0$), it has been shown theoretically [32] that the vesicle reaches a stationary state among several families of solutions, which is selected by the initial shape. In particular, two distinct families of

axisymmetric solution exist, depending on whether the initial condition is oblate or prolate. Prolate settling vesicles can adopt egg and pear-like shapes. These shapes have been observed experimentally (Fig. 2, top, of [29]) and correspond to the family of prolate shapes obtained in simulations (e.g., pear shape for Bo = 59 in Fig. 2). Oblate settling vesicles develop parachute-like shapes. Finally, nonaxisymmetric solutions also exist, which exhibit membrane recirculations [32] due to membrane fluidity, as in other cases [33,34]. Neither oblate nor nonaxisymmetric families of shapes have been reported experimentally so far. We now turn to the evolution of the system for deflated vesicles ($\Delta \sim 0.1$–1) and larger Bond numbers (Bo $\sim$ 100). This means that the interface has enough geometrical freedom to deform and that the forcing is large enough to overcome bending rigidity. In the case of an initial oblate, the parachute-like shape becomes more pronounced, but no tether appears. Thus we ignore this family in the following. In the case of an initial prolate, just after the release, the shape evolves rapidly, leading to the formation of a protrusion at the rear of the vesicle (Fig. 1). This protrusion thus elongates, and a thin tether connecting a quasispherical mother vesicle of radius R to a quasispherical daughter vesicle of radius R_2 develops (Fig. 2). The simulated shapes presented here are in qualitative agreement with recent experimental observations (Figs. 1(d) and 1(e) of [29]). However, the evolution of the shape is very sensitive to initial conditions and can lead to pearling (Fig. 1(d) of [29]), which complicates the quantitative comparison of numerical simulations with experiments due to the long time needed to reach the stationarity of the whole shape (without pearls).

Vesicles versus drops. The transient deformations corresponding to the extrusion of an elongated tether (Fig. 1) are reminiscent of the nonstationary dynamics of settling drops [35–37], yet in the case presented here, the vesicle reaches a stationary state, instead of pinch-off for drops [1,6]. To interpret the difference between the two situations, one can consider the system composed of two spheres (S and S_2) of radii R and R_2 connected by a cylindrical tether of length L and radius r. Since the settling velocity v_S for an isolated sphere of radius R in the Stokes regime is given by $v_S = 2\delta\rho g R^2/9\eta$, the quadratic dependency on the radius leads to different settling velocities for the spheres S and S_2, which elongates the tether. The force exerted at the extremities of the tether is given by the first variation of F with respect to the length,

$$\boldsymbol{f} \sim -\frac{\partial F}{\partial L}\boldsymbol{\nu} \sim -2\pi r\left(\frac{\kappa}{2r^2}+\gamma\right)\boldsymbol{\nu}, \tag{3}$$

where $\boldsymbol{\nu} = \pm\boldsymbol{e}_z$ is the unit outward pointing normal vector to the cylinder extremities. This expression is valid both for a drop (in which case $\kappa = 0$ and γ is the surface tension) and for a vesicle (in which case γ has to be determined since it is the Lagrange multiplier enforcing the surface incompressibility constraint). For a vesicle, neglecting the contribution of γ for the moment, the force varies as κ/r, which means that the tether is harder to stretch as it is elongated by the flow. To determine the value of the Lagrange multiplier in the tether, one can write the projection along the normal direction of the mechanical equilibrium of the membrane:

$$p^i - p^e + 2\gamma H - \kappa[2\Delta_s H + 4H(H^2 - K)] = 0. \tag{4}$$

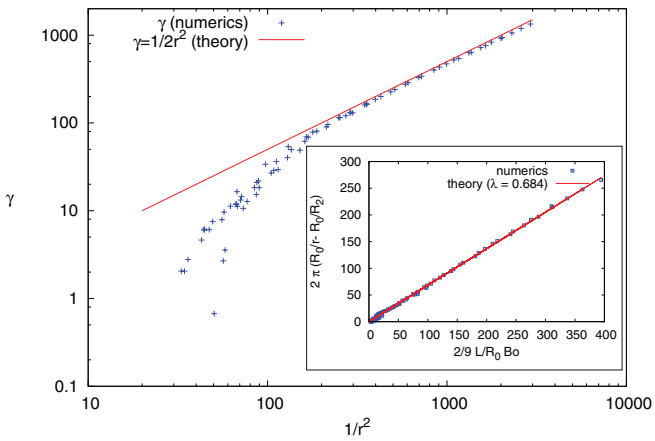

FIG. 4. (Color online) Evolution of the tension in the membrane at the junction between the tether and the mother vesicle plotted as a function of $1/r^2$, with r being the radius of the tether. The points are the values obtained with the numerical simulation, and the line is given by (5). Each of the 83 points represents a different stationary state corresponding to a different (Δ,Bo). The inset shows a comparison of the two sides of Eq. (9). The only fitting parameter, λ, sets the slope of the straight line. Equation (9) provides an estimate of the friction along the tether as a function of the variation of the radius of the tether.

The jump of pressure at the connection between the tether and the mother vesicle can be estimated by Laplace's law, $p^i - p^e = 2\gamma/R$. Thus, at leading order in $r/R \ll 1$, $H \approx -1/2r$ and Eq. (4) writes $2\gamma H \approx 4\kappa H^3$, which gives

$$\gamma \sim \kappa/2r^2. \tag{5}$$

A comparison of this scaling and of the values of the numerical simulations gives excellent agreement when the approximation $r/R \ll 1$ is valid (Fig. 4). Using it in Eq. (3) thus gives

$$\boldsymbol{f} \sim \pm 2\pi\kappa/r\ \boldsymbol{e}_z, \tag{6}$$

where the plus (minus) sign corresponds to the force exerted by the tether on sphere S (S_2). Thus the Lagrange multiplier enhances the stabilizing effect of bending.

In contrast, the expression of the force exerted by a fluid cylinder in the case of constant surface tension (drop) is

$$\boldsymbol{f} \sim \pm 2\pi\gamma r\ \boldsymbol{e}_z. \tag{7}$$

Thus, for a drop, $\boldsymbol{f}$ diminishes as the cylinder is elongated, while the situation is the opposite for a vesicle where the force grows when the radius decreases. This is the crucial stabilizing ingredient which allows for the stationarity of a tether on a vesicle while a tether on a drop is easier to stretch as it is elongated. Indeed, the first step of the dynamics is governed by bending, which stabilizes the pinch-off at the mother-tube location on a short time scale (see Fig. 1) compared to tether elongation time. Without bending energy and with membrane incompressibility, the tether length (radius) elongates (decreases) endlessly. This is surprising as a first intuitive statement would attribute the tether stationarity only to the fixed-area constraint. But, in fact, zero bending modulus corresponds to an infinite Bond number and there is no other dimensionless number in Stokes flow to balance gravity. The fixed-area constraint establishes a relationship

between the various length scales (R, R_2, L, r) while bending governs the minimal radius.

Using the conservation of excess area of the cylinder yields the force f roughly proportional to $\kappa L/\Delta R_0^2$. Thus, the cylinder acts as a spring with a stiffness given by κ/Δ. This is directly visible on Fig. 3, where the excess area is varied while the Bond number is kept constant (omitting the small variations of R and R_2, this corresponds to a constant forcing on a spring with a varying stiffness). This singular variation of the stiffness with respect to the excess area differs markedly from experiments and theory with a fixed tension Σ, in which case the area is free. In this case, an important theoretical result is that a critical force is required to pull a tether, and this force can be linked [23,24] to the fixed tension Σ by $f_c = 2\pi\sqrt{2\Sigma\kappa}$. The radius of the tether is also completely determined by Σ as $r = \sqrt{\kappa/2\Sigma}$. This corresponds to the same relation as (5) since both result from the equilibrium between tension and bending forces in the tether. However, in the case presented here, neither γ nor r is fixed as they result from the interplay between the conservation of excess area and the equilibrium of settling-induced stresses.

Role of friction. This description omits the friction forces on the tether due to hydrodynamical fields. These forces modify the tension γ on the tether (Fig. 3) and thus lead to an increase of the tether radius with a minimum at the connection to the mother vesicle, contrary to the point-like force configuration for which the minimum is at the end of the tether [19,22]. Writing the mechanical equilibrium of the tether, $-(2\pi\kappa/r)\boldsymbol{e}_z + \boldsymbol{f_2} - \lambda\eta L\boldsymbol{v} = \boldsymbol{0}$, where we assume that the friction force on the tether per unit length is given by $\lambda\eta\boldsymbol{v}$, with λ being a numerical prefactor, and $\boldsymbol{f_2}$ is the force exerted by the upper half sphere S_2. This force is estimated as the sum of the membrane and pressure contributions:

$$\boldsymbol{f_2} = 2\pi R_2\left(\gamma_2 + \frac{\kappa}{2R_2^2}\right)\boldsymbol{e}_z - \int_{S_2} p^i \boldsymbol{n} dS. \tag{8}$$

Using Laplace's law and Eq. (4) at the upper junction gives $\gamma_2 \approx -\kappa/2R_2^2$, a negative value obtained also in numerical computation. Using Fig. 3 (top panel), $R_2/R_0 \approx 0.10$, which provides a dimensionless $\gamma_2 \approx -(R_0/R_2)^2/2 \approx -50$, a good order of magnitude compared to the numerical result. The membrane contribution in Eq. (8) vanishes, and the force exerted on the tether by S_2 is due solely to the pressure. The global equilibrium of the upper half sphere leads to $\boldsymbol{f_2} \sim \pi\kappa/R_2\boldsymbol{e}_z$. Thus the mechanical equilibrium of the tether writes

$$2\pi\left(\frac{R_0}{r} - \frac{R_0}{R_2}\right) \approx \frac{2}{9}\lambda\frac{L}{R_0}\mathrm{Bo}. \tag{9}$$

This equation is plotted in the inset of Fig. 4 and shows very good agreement with a numerical prefactor given by the best fit of $\lambda = 0.684$. This has direct interest for experiments since it could allow for computation of the minimal radius using measures of the upper radius as well as the length and velocity of the tether. Experimentally, the Bond number can easily span the $[0, 5 \times 10^3]$ range, corresponding to a 10 μm radius vesicle with velocities in the 1 $\mu\mathrm{m\,s}^{-1}$ range. In the simulations reported here, a tether radius as low as 200 nm with a 45 μm length has been simulated.

To conclude, we have shown that a buoyant deflated vesicle settling in a viscous flow will develop a stationary tether at the rear of the vesicle, provided the excess area and the Bond number are large enough and the initial shape is prolate. Contrary to the point-like force configuration, this is a situation where the area of application of the external force has no meaning and the tension of the membrane is free, selected by the system. The evolution to this tethered shape from the pear-like shapes which exist at lower (Δ, Bo) is continuous (no first-order shape transition). The pulling force is due to the settling flow and can be understood as being due to a difference of settling velocities of spheres with different radii. The stationarity is due to the resistance of the tether to bending, which opposes the radius reduction due to tether stretching.

ACKNOWLEDGMENTS

This work has benefited from financial support from the ANR CAPSHYDR (Grant No. 11-BS09-013-02), from Labex MEC (Grant No. ANR-11-LABX-0092), from A*MIDEX (Grant No. ANR-11-IDEX-0001-02), and from CNES. Computations were performed at the Mésocentre d'Aix-Marseille Université. This research was supported in part by the Project of Knowledge Innovation Program (PKIP) of the Chinese Academy of Sciences, Grant No. KJCX2.YW.W10.2.

[1] X. D. Shi, M. P. Brenner, and S. R. Nagel, Science **265**, 219 (1994).
[2] I. Cohen and S. R. Nagel, Phys. Rev. Lett. **88**, 074501 (2002).
[3] S. Courrech du Pont and J. Eggers, Phys. Rev. Lett. **96**, 034501 (2006).
[4] A. Rustom, R. Saffrich, I. Markovic, P. Walther, and H.-H. Gerdes, Science **303**, 1007 (2004).
[5] D. W. Schmidtke and S. L. Diamond, J. Cell Biol. **149**, 719 (2000).
[6] Y. Amarouchene, D. Bonn, J. Meunier, and H. Kellay, Phys. Rev. Lett. **86**, 3558 (2001).
[7] Y. Shin, M. Hohman, M. Brenner, and G. Rutledge, Polymer **42**, 09955 (2001).
[8] U. Seifert, Adv. Phys. **46**, 13 (1997).
[9] P. Vlahovska, T. Podgorski, and C. Misbah, C. R. Phys. **10**, 775 (2009).
[10] M. Abkarian and A. Viallat, Soft Matter **4**, 653 (2008).
[11] H. Zhao and E. S. G. Shaqfeh, J. Fluid Mech. **674**, 578 (2011).
[12] A. Farutin and C. Misbah, Phys. Rev. Lett. **109**, 248106 (2012).
[13] M. Abkarian, C. Lartigue, and A. Viallat, Phys. Rev. Lett. **88**, 068103 (2002).
[14] H. Zhao, A. P. Spann, and E. S. G. Shaqfeh, Phys. Fluids **23**, 121901 (2011).
[15] E. Evans, H. Bowman, A. Leung, D. Needham, and D. Tirrell, Science **273**, 933 (1996).

[16] D. K. Fygenson, J. F. Marko, and A. Libchaber, Phys. Rev. Lett. **79**, 4497 (1997).
[17] M. Karlsson, K. Sott, M. Davidson, A.-S. Cans, P. Linderholm, D. Chiu, and O. Orwar, Proc. Natl. Acad. Sci. USA **99**, 11573 (2002).
[18] A. Roux, G. Cappello, J. Cartaud, J. Prost, B. Goud, and P. Bassereau, Proc. Natl. Acad. Sci. USA **99**, 5394 (2002).
[19] O. Rossier, D. Cuvelier, N. Borghi, P. H. Puech, I. Derényi, A. Buguin, P. Nassoy, and F. Brochard-Wyart, Langmuir **19**, 575 (2003).
[20] J.-M. Allain, C. Storm, A. Roux, M. Ben Amar, and J.-F. Joanny, Phys. Rev. Lett. **93**, 158104 (2004).
[21] G. Koster, A. Cacciuto, I. Derényi, D. Frenkel, and M. Dogterom, Phys. Rev. Lett. **94**, 068101 (2005).
[22] F. Brochard-Wyart, N. Borghi, D. Cuvelier, and P. Nassoy, Proc. Natl. Acad. Sci. USA **103**, 7660 (2006).
[23] I. Derényi, F. Jülicher, and J. Prost, Phys. Rev. Lett. **88**, 238101 (2002).
[24] T. R. Powers, G. Huber, and R. E. Goldstein, Phys. Rev. E **65**, 041901 (2002).
[25] N. Shahidzadeh, D. Bonn, O. Aguerre-Chariol, and J. Meunier, Phys. Rev. Lett. **81**, 4268 (1998).
[26] P. Marmottant, T. Biben, and S. Hilgenfeldt, Proc. R. Soc. A **464**, 1781 (2008).
[27] V. Kantsler, E. Segre, and V. Steinberg, Phys. Rev. Lett. **101**, 048101 (2008).
[28] S. Chatkaew, M. Georgelin, M. Jaeger, and M. Leonetti, Phys. Rev. Lett. **103**, 248103 (2009).
[29] Z.-H. Huang, M. Abkarian, and A. Viallat, New J. Phys. **13**, 035026 (2011).
[30] H. Zhao and E. S. G. Shaqfeh, J. Fluid Mech. **719**, 345 (2013).
[31] G. Boedec, M. Leonetti, and M. Jaeger, J. Comput. Phys. **230**, 1020 (2011).
[32] G. Boedec, M. Jaeger, and M. Leonetti, J. Fluid Mech. **690**, 227 (2012).
[33] G. Coupier, A. Farutin, C. Minetti, T. Podgorski, and C. Misbah, Phys. Rev. Lett. **108**, 178106 (2012).
[34] F. G. Woodhouse and R. E. Goldstein, J. Fluid Mech. **705**, 165 (2012).
[35] C. J. Koh and L. G. Leal, Phys. Fluids A **1**, 1309 (1989).
[36] C. J. Koh and L. G. Leal, Phys. Fluids A **2**, 2103 (1990).
[37] C. Pozrikidis, J. Fluid Mech. **210**, 1 (1990).